

# Spatial damping identification in the frequency domain - a theoretical and experimental comparison

Matija Brumat, Janko Slavič, Miha Boltežar  
University of Ljubljana, Faculty of Mechanical Engineering,  
Laboratory for dynamics of machines and structures,  
Aškerčeva 6, 1000 Ljubljana, SI, Slovenia

May 26, 2016

**Cite as:**

**Matija Brumat, Janko Slavič and Miha Boltežar**  
**Spatial damping identification in the frequency domain – A Theoretical and**  
**Experimental Comparison.**  
**Journal of Sound and Vibration, 376:182 – 193, 2016**  
**DOI: 10.1016/j.jsv.2016.04.006**

**Abstract**

This paper deals with spatial damping identification methods. In contrast to the commonly used damping methods (modal, proportional) the spatial damping information improves structural models with a known location of the damping sources. The Lee-Kim, Chen-Ju-Tsuei, Fritzen IV and local equation of motion methods were theoretically and experimentally compared. Experimentally, the spatial damping identification was tested against: modal and spatial incompleteness, differences in viscous and hysteretic damping models, the performance of identification methods and the effect of damping treatments. It was found that for a structure with a known equation of motion (beam, plate) the local equation of motion method is more efficient and gives a more precise location of the damping. Full frequency response function (FRF) matrix methods can also identify the spatial damping, but are more demanding because the numerical and measurement effort increases with  $n^2$ , where  $n$  is the number of measurement points and, consequently, the size of the FRF matrix.

# 1 Introduction

Damping, combined with mass and stiffness, represents the dynamic properties of a structure, and its identification is important for validating and building analytical/numerical models in civil, mechanical and aerospace engineering. Damping in linear mechanical systems is normally identified using a method such as logarithmic decay [1] in the time domain, the continuous wavelet transform [2] and the Morlet wave [3] in the time-frequency domain or the half-power point [1], the closed-form solution [4] and the first-order perturbation [5] in the frequency domain. In the modal domain the Error Matrix Method was extended to locate the damping sources on the structure [6]. However, most of the described methods can be applied to viscous damping, only. Examples, where an exact damping spatial location is needed, are: the identification of damping sources on existing structures and the precise application of a damping treatment. However, the typically used damping-identification methods [1, 7] do not provide spatial information (damping distribution throughout the structure).

An alternative approach is to use direct damping-identification methods that were developed for the identification of the damping distribution directly from the frequency-response functions (FRFs) without a transformation to the modal coordinates. The first is the widely used Fritzen IV method [9], where IV stands for Instrumental Variable. Instrumental variable methods were developed for an unbiased estimation of the model parameters [9, 10] in comparison with least-squares methods, which are biased due to the noisy measurement data [9]. In 1996 Chen *et al.* presented a method [11] that identifies the damping separately from the mass and stiffness based on the imaginary and the real properties of the FRF. A simplified version of the Chen, Ju and Tsuei's [11] method is Lee and Kim's dynamic stiffness method [12] (it requires only one matrix inverse, resulting in a smaller error). To improve the damping identification on real structures Arora *et al.* [13] proposed a two-step procedure. In the first step, the mass and stiffness matrices are updated using FRF data, and in the second step, the damping matrix is identified using updated mass and stiffness matrices from the previous step. The two-step approach relates the displacements to the material properties, which can also be made using the local equation of motion method [14], presented recently by Ablitzer *et al.* Some direct methods, not considered in this research, are reviewed in [4, 5, 15].

Besides a theoretical and experimental comparison of the methods, this research focuses on the experimental effects of: the modal incompleteness, the spatial incompleteness and the damping model. Modal incompleteness deals with the limited frequency span over the number of modes, whereas the spatial incompleteness covers the effects of the non-measured points on the structure. Modal and spatial incompleteness for spatial damping have been studied numerically [5, 16] and experimentally [15] on low-DOF models.

## 2 Theoretical background

In this section the background to the direct damping identification methods is briefly presented [1]. Each method will be presented for both types of the most common linear-damping models: the viscous and the hysteretic.

In contrast to the viscous damping model, one must be careful when using a hysteretic model as it does not satisfy the causality requirement [17, 18]. Further details are given in [19].

The starting point for the frequency-based, direct-damping identification methods is the frequency response function (FRF) matrix  $\mathbf{H}(\omega)$ . Assuming a viscous linear system and harmonic excitation/response at frequency  $\omega$ , the general second-order equation of motion with the viscous damping can be written in the frequency domain as:

$$[\mathbf{K} - \omega^2 \mathbf{M} + i\omega \mathbf{C}] \mathbf{X}(\omega) = \mathbf{F}(\omega) \quad (1)$$

where  $\mathbf{M}$  is the mass matrix,  $\mathbf{C}$  is the viscous-damping matrix and  $\mathbf{K}$  is the stiffness matrix. The remaining parts of (1) are the imaginary unit  $i^2 = -1$ , the Fourier transforms of the response

$\mathbf{X}(\omega)$  and the force vector  $\mathbf{F}(\omega)$ . From Eq. (1), the FRF matrix  $\mathbf{H}(\omega)$  is defined as:

$$\mathbf{X}(\omega) = \mathbf{H}(\omega) \mathbf{F}(\omega) \quad (2)$$

and furthermore:

$$\mathbf{H}(\omega) = [\mathbf{K} - \omega^2 \mathbf{M} + i\omega \mathbf{C}]^{-1} \quad (3)$$

The dynamic stiffness matrix  $\mathbf{Z}(\omega)$  is defined as the matrix inverse of  $\mathbf{H}(\omega)$  for each frequency point  $\omega$ :

$$\mathbf{Z}(\omega) = \mathbf{H}(\omega)^{-1} = [\mathbf{K} - \omega^2 \mathbf{M} + i\omega \mathbf{C}] \quad (4)$$

Chen et al. [11] also define the undamped or “normal” FRF  $\mathbf{H}_N(\omega)$  as:

$$\mathbf{H}_N(\omega) = [\mathbf{Z}_N(\omega)]^{-1} = [\mathbf{K} - \omega^2 \mathbf{M}]^{-1} \quad (5)$$

## 2.1 Chen, Ju and Tsuei’s method

The method proposed by Chen *et al.* (1996) [11] identifies the damping matrix in a separate step from the stiffness  $\mathbf{K}$  and mass  $\mathbf{M}$  matrix using measurements based on the imaginary and real properties of the FRF as follows. The general equation of motion Eq. (1) can then be written as a combination of the normal FRF  $\mathbf{H}_N(\omega)$  and the damping:

$$[\mathbf{H}_N(\omega)]^{-1} \mathbf{X}(\omega) + i\omega \mathbf{C} \mathbf{X}(\omega) = \mathbf{F}(\omega) \quad (6)$$

Multiplying both sides of Eq. (6) by  $\mathbf{H}_N(\omega)$  from the left gives:

$$\mathbf{X}(\omega) + i\omega \mathbf{H}_N(\omega) \mathbf{C} \mathbf{X}(\omega) = \mathbf{H}_N(\omega) \mathbf{F}(\omega) \quad (7)$$

Defining the transformation matrix  $\mathbf{T}(\omega)$ :

$$\mathbf{T}(\omega) = \omega \mathbf{H}_N(\omega) \mathbf{C} \quad (8)$$

and recalling that  $\mathbf{X}(\omega) = \mathbf{H}(\omega) \mathbf{F}(\omega)$ , Eq. (7) can be simplified to:

$$\mathbf{H}_N(\omega) = [\mathbf{I} + i\mathbf{T}(\omega)] \mathbf{H}(\omega) \quad (9)$$

The real and imaginary parts of Eq. (9) are then rewritten separately:

$$\begin{aligned} \mathbf{H}_N(\omega) &= [\text{Re}(\mathbf{H}(\omega)) - \mathbf{T}(\omega) \text{Im}(\mathbf{H}(\omega))] \\ &\quad + i[\mathbf{T}(\omega) \text{Re}(\mathbf{H}(\omega)) + \text{Im}(\mathbf{H}(\omega))] \end{aligned} \quad (10)$$

The transformation matrix  $\mathbf{T}(\omega)$  and the normal FRF matrix  $\mathbf{H}_N(\omega)$  are real by definition; therefore, it follows that the imaginary part of Eq. (10) equals  $\mathbf{0}$ :

$$\begin{aligned} \text{Im}(\mathbf{H}_N(\omega)) &= \mathbf{0} \\ &= [\mathbf{T}(\omega) \text{Re}(\mathbf{H}(\omega)) + \text{Im}(\mathbf{H}(\omega))] \end{aligned} \quad (11)$$

From Eq. (11) it is clear that the transformation matrix  $\mathbf{T}(\omega)$  can be defined only with the matrix  $\mathbf{H}(\omega)$ :

$$\mathbf{T}(\omega) = -\text{Im}(\mathbf{H}(\omega)) [\text{Re}(\mathbf{H}(\omega))]^{-1} \quad (12)$$

The remaining real part of Eq. (10) defines the relationship between the normal and the measured FRF matrix:

$$\mathbf{H}_N(\omega) = \text{Re}(\mathbf{H}(\omega)) - \mathbf{T}(\omega) \text{Im}(\mathbf{H}(\omega)) \quad (13)$$

With the measured  $\mathbf{H}(\omega)$ , the transformation matrix  $\mathbf{T}$  can be identified. Consequently, from Eq. (8) the damping matrix can also be identified as:

$$\mathbf{C} = -\frac{1}{\omega} [\mathbf{H}_N(\omega)]^{-1} [\text{Im}(\mathbf{H}(\omega)) [\text{Re}(\mathbf{H}(\omega))]^{-1}] \quad (14)$$

A similar procedure would result in the identification of the hysteretic damping matrix [20]:

$$\mathbf{D} = -[\mathbf{H}_N(\omega)]^{-1} [\text{Im}(\mathbf{H}(\omega)) [\text{Re}(\mathbf{H}(\omega))]^{-1}] \quad (15)$$

## 2.2 Lee and Kim's method

Lee and Kim (2001) [12] suggested a simpler procedure than Chen, Ju and Tsuei's method, with only one matrix inverse for a more numerical error-prone identification. Using Eq. (4) the viscous damping matrix can be obtained directly from the imaginary part of the dynamic stiffness matrix  $\mathbf{Z}(\omega)$ :

$$\text{Im}(\mathbf{Z}(\omega)) = \text{Im}([\mathbf{H}(\omega)]^{-1}) = \omega \mathbf{C}, \quad (16)$$

Rearranging Eq. (16) to isolate the viscous-damping matrix  $\mathbf{C}$  gives:

$$\mathbf{C} = \frac{1}{\omega} \text{Im}([\mathbf{H}(\omega)]^{-1}) \quad (17)$$

Method is not limited to the viscous damping [21], for example, the hysteretic-damping matrix version of Eq. (17) is:

$$\mathbf{D} = \text{Im}([\mathbf{H}(\omega)]^{-1}) \quad (18)$$

## 2.3 Instrumental variable method

The instrumental variable (IV) method is used to estimate the causal relationships in econometrics [5]; Fritzen (1986) [9] applied the method to structural dynamics. From Eq. (4) it follows that multiplying the FRF matrix  $\mathbf{H}(\omega)$  by the dynamic stiffness  $\mathbf{Z}(\omega)$  results in the identity matrix  $\mathbf{I}$ . With a measured  $\mathbf{H}(\omega)$ , the error  $\mathbf{E}(\omega)$ :

$$\mathbf{H}(\omega) \mathbf{Z}(\omega) = \mathbf{I} + \mathbf{E}(\omega) \quad (19)$$

can therefore be minimised for the structural parameter ( $\mathbf{M}$ ,  $\mathbf{K}$ ,  $\mathbf{C}$ ,  $\mathbf{D}$ ) identification via the dynamic stiffness  $\mathbf{Z}(\omega)$  Eq. (4):

$$\mathbf{Z}(\omega) = [-\omega^2 \mathbf{M} + i\omega \mathbf{C} + \mathbf{K}] = [-\omega^2 \mathbf{I} \quad i\omega \mathbf{I} \quad \mathbf{I}] \begin{bmatrix} \mathbf{M} \\ \mathbf{C} \\ \mathbf{K} \end{bmatrix} \quad (20)$$

Combining Eq. (19) and Eq. (20) gives:

$$\underbrace{[-\omega^2 \mathbf{H}(\omega) \quad i\omega \mathbf{H}(\omega) \quad \mathbf{H}(\omega)]}_{\mathbf{A}(\omega)} \underbrace{\begin{bmatrix} \mathbf{M} \\ \mathbf{C} \\ \mathbf{K} \end{bmatrix}}_{\mathbf{P}} = \mathbf{I} + \mathbf{E}(\omega) \quad (21)$$

The structural parameters  $\mathbf{P}$  are estimated from Eq. (21) as:

$$\mathbf{P} = [\mathbf{A}(\omega)]^{-1} (\mathbf{I} + \mathbf{E}(\omega)) = [\mathbf{A}(\omega)]^{-1} \mathbf{I} + [\mathbf{A}(\omega)]^{-1} \mathbf{E}(\omega) \quad (22)$$

where  $[\mathbf{A}(\omega)]^{-1} \mathbf{E}(\omega)$  represents the systematic error (bias) in the parameter estimation. For an unbiased estimation of  $\mathbf{P}$  we now define a new variable named the instrumental variable  $\mathbf{IV}$ ,

which is correlated with  $\mathbf{P}$  and uncorrelated with the systematic errors [9] and has the following properties:

$$\text{plim}_{p \rightarrow \infty} \left\{ \frac{1}{p} \mathbf{IV}^T \mathbf{E} \right\} = \mathbf{0} \quad \text{and nonsingular} \quad (23)$$

where plim denotes probability limit and  $p$  is the number of measurements. Eq. (23) implies that the bias is reduced to zero  $\mathbf{IV}^T \mathbf{E} = \mathbf{0}$  if the estimation is made using a large number of measurement points. To continue, the error  $\mathbf{E}$  is isolated from Eq. (21) and both sides have to be multiplied by instrumental variable  $\mathbf{IV}^T$ :

$$\mathbf{IV}^T \mathbf{E}(\omega) = \mathbf{IV}^T \bar{\mathbf{I}} - \mathbf{IV}^T \mathbf{A}(\omega) \mathbf{P} \quad (24)$$

Taking account of the definition Eq. (23), the left-hand side of Eq. (24) equals  $\mathbf{0}$ . The structural parameters  $\mathbf{P}$  are finally estimated from Eq. (24):

$$\mathbf{P} = \left[ \mathbf{IV}^T \mathbf{A}(\omega) \right]^{-1} \mathbf{IV}^T \bar{\mathbf{I}} \quad (25)$$

The choice of instrumental variable is open to the user; Fritzen [9] and Phani and Woodhouse [15] recommend using a reconstructed FRF Eq. (2) from the matrices ( $\mathbf{M}$ ,  $\mathbf{C}$  and  $\mathbf{K}$ ), identified using Chen, Ju and Tsuei's or Lee and Kim's method  $\mathbf{IV}(\omega) = \mathbf{H}(\omega)^{\text{reconstructed}}$ . The iterative form of Fritzen's IV method (to use the identified parameters for the next step instrumental variable) improves the parameter estimation [9, 15] and can be regarded as an iterative version of Lee and Kim's method with a predefined convergence criterion [5]. For the hysteretic version of the method the hysteretic damping  $i\mathbf{D}$  instead of the viscous damping part  $i\omega\mathbf{C}$  should be used in the respective equations.

## 2.4 Local equation of motion method

The method recently presented by Ablitzer *et al.* [14] is, in this paper, extended for beam structures and for viscous damping. The equation of motion for the displacement response  $w$  of an isotropic Euler-Bernoulli beam with hysteretic damping in the steady state is [22]:

$$\rho A \frac{\partial^2 w}{\partial t^2} + E(1 + i\eta) I \frac{\partial^4 w}{\partial x^4} = f(x, t) \quad (26)$$

where  $\rho$  is the density,  $A$  is the cross-section,  $E$  is the elastic modulus,  $\eta$  is the hysteretic damping ratio,  $I$  is the second moment of area and  $f(x, t)$  is the point harmonic excitation force at the frequency  $\omega$ , respectively. The viscous damping [23] equation differs only slightly:

$$\rho A \frac{\partial^2 w}{\partial t^2} + E I \frac{\partial^4 w}{\partial x^4} + \gamma \frac{\partial w}{\partial t} = f(x, t) \quad (27)$$

where  $\gamma$  is the viscous damping constant per unit length. the harmonic response  $w(x, t)$  can be written using the method of separation of variables as:

$$w(x, t) = W(x) \sin(\omega t) \quad (28)$$

where  $W$  is response of the beam and is only dependent on the position on the beam  $x$ . The designation of the dependency on  $x$  will be omitted from here on for reasons of clarity. The partial time derivatives in Eq. (26) and Eq. (27) can then be expressed as:

$$\frac{\partial^2 w}{\partial t^2} = -\omega^2 W \sin(\omega t) \quad (29)$$

and:

$$\frac{\partial w}{\partial t} = i\omega W \sin(\omega t) \quad (30)$$

The fourth derivative is approximated at the measurement point  $j$  by the finite-difference scheme  $\delta_j^4$ :

$$\frac{\partial^4 w}{\partial x^4} = \delta_j^4 \sin(\omega t) \quad (31)$$

$$\delta_j^4 = \frac{1}{\Delta_x^4} (W_{j+2} - 4W_{j+1} + 6W_j - 4W_{j-1} + W_{j-2}) \quad (32)$$

where  $\Delta_x$  is the measurement mesh spacing. Combining Eq. (26) with Eq. (29) and Eq. (31) for the measurement point  $j$  we obtain:

$$-\rho A \omega^2 W_j \sin(\omega t) + E_j(1 + i\eta_j) I \delta_j^4 \sin(\omega t) = f(x_j, t) \quad (33)$$

When the excitation is applied outside the observation area (Fig. 1), the right-hand side of Eq. (33) is  $f(x_j, t) = 0$  and Eq. (33) can be separated into real and imaginary parts:

$$E_j = \frac{\rho A \omega^2}{I} \operatorname{Re} \left[ \frac{W_j}{\delta_j^4} \right] \quad (34)$$

$$\eta_j = \frac{\rho A \omega^2}{E I} \operatorname{Im} \left[ \frac{W_j}{\delta_j^4} \right] \quad (35)$$

For a viscous system the real part is the same as in Eq. (34) and the damping per unit length  $\gamma_j$  at the measurement point  $j$  is:

$$\gamma_j = -\frac{E_j I}{\omega} \operatorname{Im} \left[ \frac{\delta_j^4}{W_j} \right] \quad (36)$$

The discrete viscous damping  $c_j$  is obtained from the damping per unit length  $\gamma_j$  as:

$$c_j = \gamma_j \Delta_x \quad (37)$$

The presented approach is straightforward to use, but better results due to measurement-noise amplification in the fourth-order derivation can be obtained with a two-step regularization [14]. First, both fields  $\delta_j^4$  and  $W_j$  are multiplied by a spatial Tukey window for the boundary-effects attenuation and in the second step each field is convolved with the discrete spatial response of a low-pass filter. The width of the filter kernel is defined by the spatial cut-off wavelength  $\lambda_c$ , e.g.,  $\lambda_c = 50$  mm, details are given in [14].

### 3 Experiments

An experiment was conducted on the three equal-sized, free-free, beam specimens to compare the direct-damping identification methods. The specimens are: a) a plain beam - beam A, b) with an asymmetrically added local viscous damper - beam B and c) with a constrained layer damping (CLD) - beam C, see Fig. 2. The beam specimens B and C have an asymmetrically applied damping treatment over a restricted area of the beam in order to know the damping spatial location. Three samples were considered to emphasize the effect of the different damping treatments on the identified spatial location in the subsequent discussion.

#### 3.1 Plain free-free beam

The beam A was a plain steel beam with a constant cross-section  $h \times b = 1 \text{ mm} \times 30 \text{ mm}$ , length  $l = 400 \text{ mm}$ , mass  $m = 92.6 \text{ g}$  and Young's modulus  $E = 210000 \text{ MPa}$ . The beam dimensions were selected to have a low modal overlap and to have a large number of modes in the frequency span up to 3000 Hz. The beam is shown in Fig. 2(a). Two soft springs (stiffness  $\approx 50 \text{ N/m}$ ) were used at each beam boundary in the y-direction to limit the rigid-body translation after the impact.

### 3.2 Free-free beam with added discrete viscous damper

The beam B was a similar steel beam to beam A, but an additional viscous damper was added between points 5 and 8, see Fig. 2(b). The discrete damper is based on the design of Rijnen *et. al.* [24], with each damper being made from two rubber blocks of size 5x5x1 mm glued with cyanoacrylate to the beam and connected with aluminium struts of size 80x5x5 mm.

### 3.3 Free-free beam with added constrained layer damper

The beam C was the steel beam used as beam A, but it had attached a constrained layer damper, as shown in Fig. 2(c). The visco-elastic layer for the application was 3M 112P02 damping material [25]. The steel constraining layer was of the same material and thickness as the beam in order to maximize the damping [25]. Holes were drilled in the constraining layer to measure the responses of the beam, only.

### 3.4 Measurement setup

The measurement setup is shown in Fig. 3. A custom-made solenoid impactor with a PCB 086E80 force sensor was used for the repeatable impulse excitation (described later). The response (velocity) measurements employed a Polytec PDV100 laser vibrometer. The impactor/laser-based measurement allows for a non-contact measurement without any structural modification due to the added stiffness or mass from the sensors or shakers. The data acquisition and the signal processing were undertaken in the custom python software environment using the pyDAQmx library [26] to interface with the NI 9215 acquisition hardware. The sampling rate was 100 kHz and the signal was captured for 10 seconds. Other details considered during the experiment are:

- The structure is sequentially excited at 15 points and responses are measured at the same 15 points in the  $y$  direction (15x15 excitation-response pairs,  $n = 15$ ), as shown in Fig 3
- For the local equation of motion method (see Section 2.4) a denser measurement mesh is needed due to the fourth-order spatial differentiation and subsequent filtering, see Eq. (32). The structure was excited at point 15 and between points 3 and 11 an additional 100, equally spaced, responses were measured to obtain the 2.5-mm-measurement mesh.
- Internal low- and high-pass filters in the PDV100 vibrometer were set to 22 kHz and 0.1 Hz, respectively [27].
- The instrumentation phase error was compensated using the time-shift approach from [15]
- Each excitation-response point was measured three times to obtain the averaged  $H_1$  estimator (mobility FRF).
- The mobility FRFs were divided by  $i\omega$  in the frequency domain to obtain the receptance FRFs [1].

#### 3.4.1 Solenoid impactor

The solenoid impactor is based on the designs of [28, 29] and is built using a 24-V push-type solenoid with a 30-mm diameter. For a faster acceleration of the solenoid core and thus the impact force, the solenoid should be driven at a higher voltage (due to the solenoid's winding inductance). The impact is triggered using a microcontroller-based MOSFET switch with a microsecond resolution. For a 40-V supply a solenoid needs 5 milliseconds of open switch to travel 5 mm and impacts with a 14-N peak force and a duration of approximately 0.15 ms, see Fig. 4.

## 4 Analysis and discussion

For each beam 675 (225 points with 3 averages) measured responses were assembled into a full FRF matrix of size  $15 \times 15$ , used by the direct damping identification methods. Fig. 5 shows an example of the measured receptance magnitude FRF at the pair 15-10 for all three beams; where 15-10 denotes the 15th excitation and the 10th response point (this designation will be used throughout the paper). From the FRFs it is clear that the damping treatment of beams B and C affects the high-frequency region more than the low-frequency region. Furthermore, the added stiffness and the mass due to the damping treatment barely shift the eigenfrequencies, see Fig. 5.

In contrast to the damping amplitudes at the eigenfrequencies, the damping spatial location is the focus of this research. Before using viscous and hysteretic damping matrix identification methods, the measured FRFs have to be tested for repeatability, linearity and most importantly for FRF reciprocity. For a damping model with a symmetric damping matrix the reciprocity is expected [30]. Nevertheless, the measured FRFs deviate from reciprocity in some details (see Fig. 6), which is often the case in experimental measurements [15, 31]. The observed deviations of the reciprocity can be eliminated using FRF matrix symmetrisation at every frequency point using [32]:

$$\mathbf{H}(\omega) = 0.5 [\mathbf{H}(\omega) + \mathbf{H}^T(\omega)] \quad (38)$$

Any non-symmetry in the identified damping matrices after this step is due to the identification procedure only.

### 4.1 Modal incompleteness

The modal incompleteness is presented in detail using the Lee-Kim method, see Eq. (17). Fig. 7 shows the absolute values of the identified viscous damping matrix  $\mathbf{C}$  for beam B using a frequency range of five (0-200 Hz), ten (0-1100 Hz) and fifteen modes (0-3000 Hz). The larger numerical values (e.g. 150 Ns/m in Fig. 7) represent areas of higher damping. The identified matrices are symmetric.

Focusing on the identified values in Fig. 7 reveals higher damping values at the points of the applied damping for beam B (left point 4 and right point 9 of the discrete damper).

Comparing the high modal incompleteness with the low incompleteness model it is clear that the spatial location of the damping becomes localised when the modal incompleteness is sufficiently low, see Fig. 7. The frequency range of at least ten modes should be used for an accurate viscous damping location - similar conclusions were found in a theoretical study [16].

A theoretical explanation for the modal incompleteness on the identification of the spatial damping matrix  $\mathbf{C}$  seen in Fig. 7 is given in [33, 34, 16]. The authors conclude that it is impossible to identify the structural parameters of a real mechanical system from a FRF matrix, measured over a limited frequency range.

Modal incompleteness affects the Chen-Ju-Tsuei and Fritzen methods in a similar way to the Lee-Kim method, as all three methods are based on the complex properties of the FRF function, but for reasons of brevity the details are not provided here. The local equation of motion method requires a different analysis and will be discussed later.

### 4.2 Spatial incompleteness

The spatial incompleteness test was made using the full FRF matrix (15 modes) with deleted rows and columns. These deleted rows and columns can be understood as degrees of freedom (DOF) that were not measured (columns represent response DOFs and rows represent excitation DOFs).

Fig. 8 shows the identified matrix using the Lee-Kim method for four DOFs (i.e., 1, 5, 10, 15) and eight DOFs (i.e., 1, 3, 5, 7, 9, 11, 13, 15). Comparing the results for the 15 modes shown in Fig. 7 with Fig. 8 the redistribution of damping over the neighbouring spatial location is observed. The high damping area around the pair 4-9 in Fig. 7 (15 modes) is in the spatially incomplete cases redistributed because of the missing information. In the case of 8 DOF the redistribution

is to the pair 5-11 and in case of 4 DOF over the complete damping matrix. Low DOF models also tend to have larger damping values because the amount of damping present in the structure is redistributed over fewer DOFs.

The spatial incompleteness is related to the modal incompleteness [33, 34, 16], e.g., from the experimental modal analysis it is clear that the number of extracted mode shapes depends on the FRF matrix  $\mathbf{H}(\omega)$  shape.

### 4.3 Viscous vs. hysteretic damping

Fig. 9 shows the absolute values of the identified hysteretic damping matrix of beam B using the hysteretic Lee-Kim method (Eq. 18) for a frequency span of 15 modes. The identified damping distribution is similar to the viscous one, see the 15 modes result in Fig. 7.

If the comparison with the classic approach using hysteretic proportional damping [1] is made, the damping values close to the pair 4-9 are approximately 10 % (whereas the other points are 2 %) of the stiffness value for the same coordinate. The identified hysteretic damping values could be approximated as the fractions of the stiffness  $\mathbf{D} = \beta_{10} \mathbf{K}_{10} + \beta_2 \mathbf{K}_2$ , where  $\beta_p$  is the proportional damping factor,  $p$  is the damping value index and  $\mathbf{K}_p$  is the stiffness matrix of the non-zero elements over the points of different damping values.

The localisation performance of the identification method is independent of the choice between the hysteretic and the viscous model. The advantage of using the hysteretic model over the viscous thus lies in its ability to be approximated with the stiffness matrix, but care must be taken as the model does not satisfy the causality requirement [17, 18].

### 4.4 Identification methods

In this section the Lee-Kim (Eq. 17), Chen-Ju-Tsuei (Eq. 14), Fritzen IV (Eq. 25) and the local equation of motion method (Eq. 36) are compared. Fig. 10 shows the identified viscous damping matrix (frequency span of 15 modes) for the Chen-Ju-Tsuei and Fritzen IV method and Fig. 11 for the local equation of motion method. The Lee-Kim and Chen-Ju-Tsuei methods give comparable results with regards to values and locations. On the other hand, the Fritzen IV method gives damping values of the same order, but the damping locations around the left point - 5 on the beam B are distorted. The identified damping matrix  $\mathbf{C}$  of the Fritzen IV method is also more robust with respect to noise than the Lee-Kim and Chen-Ju-Tsuei method (e.g., the values at the points outside the damped region close to zero - no damping there). Similar conclusions were found in [15]

A direct comparison of the results from Fig. 10 with the local equation of motion is not possible; the result of the local equation of motion method is not the damping matrix  $\mathbf{C}$ , but the local damping value at each measuring point. The damping is also identified at the selected frequency, only.

Fig. 11 shows the identified damping with the local equation of motion method for the frequencies 1150, 1840 and 3100 Hz with a spatial cut-off of  $\lambda_c = 20$  mm at the location between 30 and 240 mm of the discretely damped beam - B. Higher damping values can be found at 120 mm and at 200 mm (location of the discrete damper), see Fig. 2. The lower frequencies are more contaminated with noise (locations 50-100 mm).

If the structure has a known equation of motion (plate, beam) then the local equation of motion method can be used as it is more robust with respect to modal and spatial incompleteness (due to the required finer measurement mesh and the easier measurement procedure for obtaining a large number of responses). On the other hand, full FRF matrix-identification methods do not require any a-priori knowledge about the structure under investigation.

### 4.5 Effect of damping treatment on the spatial location

In this section the Lee-Kim method for a frequency span of 15 modes is used to evaluate the different damping treatments. The identified viscous damping matrix for beam B was already

shown in Fig. 7 - 15 modes. The identified viscous matrices for the remaining two beams are shown in Fig. 12. On the plain beam A there are higher damping values identified at the points corresponding to the beam boundaries, where the beam was suspended and an additional soft spring was attached, i.e., at 1-1 and 15-15. The identified damping values of the non-boundary points for beam A are two orders of magnitude lower than for beam C with the CLD treatment. Beam C has more pronounced damping values around points 5-8, which corresponds to the location of the constraining layer damping treatment. The identified damping matrices of beams A and C are also symmetric.

The relationship between the physical location of the damping treatment and the location of the damping values in the identified damping matrix is not always straightforward (example of the identified damping of the beams B and C, see Fig. 7 and Fig. 12). The major damping values occur close to the main matrix diagonal.

## 5 Conclusion

The effectiveness of an experimental, viscous-damping, spatial location identification was analysed. A special measuring setup was employed to measure the full FRF matrix of size  $15 \times 15$  for three different beam configurations (plain and with discrete and constrained layer damping treatments). The following conclusions can be drawn:

- In the experiment a frequency range of 10 modes is sufficient for the spatial location identification on the beam, similar to the theoretical findings of Prandina *et. al.* [16].
- The identified viscous and hysteretic damping matrices have similar spatial distributions.
- Lee-Kim, Chen-Ju-Tsuei, Fritzen-IV and the local equation of motion methods are able to identify the damping spatial distribution for discrete, plain and constrained layer damped beam configurations. The damping spatial location of the CLD treatment differs significantly from the discretely damped (even if it was applied at the same locations).

If the structure has a known equation of motion (plate, beam) then the local equation of motion method is more efficient and gives a more precise location of the damping. Full FRF matrix methods can identify the spatial damping, but are more demanding because the numerical and measuring effort increases by  $n^2$ , where  $n$  is the number of measuring points and consequently the size of the FRF matrix.

## 6 Acknowledgements

The financial support of the Young Researchers Programme provided by the Slovenian Research Agency is gratefully acknowledged.

## References

- [1] D.J. Ewins. *Modal testing: theory, practice and application*, 2<sup>nd</sup> ed. Research Studies Press, 2000.
- [2] J. Slavič, I. Simonovski, and M. Boltežar. Damping identification using a continuous wavelet transform: application to real data. *Journal of Sound and Vibration*, 262(2):291–307, 2003.
- [3] J. Slavič and M. Boltežar. Damping identification with the Morlet-wave. *Mechanical Systems and Signal Processing*, 25(5):1632–1645, 2011.
- [4] D.F. Pilkey and D.J. Inman. A survey of damping matrix identification. In *16th International Modal Analysis Conference*. SEM, 1998.

- [5] A. Srikantha Phani and J. Woodhouse. Viscous damping identification in linear vibration. *Journal of Sound and Vibration*, 303(3–5):475 – 500, 2007.
- [6] J. He *Identification of structural dynamic characteristics*. Ph.D. thesis, Department of Mechanical Engineering Imperial College, London, 1987.
- [7] M.I. Friswell and J.E. Mottershead. *Finite Element Model Updating in Structural Dynamics*. Kluwer, 1995.
- [8] J.E. Mottershead, M. Link, and M.I. Friswell. The sensitivity method in finite element model updating: A tutorial. *Mechanical Systems and Signal Processing*, 25(7):2275–2296, 2011.
- [9] C.P. Fritzen. Identification of mass and stiffness matrices of mechanical system. *Transaction of ASME, Journal of Vibration, Acoustics, Stress and Reliability in Design*, 108:9–16, 1986.
- [10] J.E. Mottershead and C.D. Foster. An instrumental variable method for the estimation of mass, stiffness and damping parameters from measured frequency response functions. *Mechanical Systems and Signal Processing*, 2(4):379–390, 1988.
- [11] S.Y. Chen, M.S. Ju, and Y.G. Tsuei. Estimation of Mass, Stiffness and Damping Matrices from Frequency Response Functions. *Transaction of ASME, Journal of Vibration and Acoustics*, 118:78–82, 1996.
- [12] J.-H. Lee and J. Kim. Development and Validation of a New Experimental Method to Identify Damping Matrices of a Dynamic System. *Journal of Sound Vibration*, 246:505–524, 2001.
- [13] V. Arora, S.P. Singh, and T.K. Kundra. Finite element model updating with damping identification. *Journal of Sound and Vibration*, 324(3–5):1111 – 1123, 2009.
- [14] F. Ablitzer, C. Pézerat, J.-M. Génevaux, and J. Bégué. Identification of stiffness and damping properties of plates by using the local equation of motion. *Journal of Sound and Vibration*, 333(9):2454–2468, 2014.
- [15] A. Srikantha Phani and J. Woodhouse. Experimental identification of viscous damping in linear vibration. *Journal of Sound and Vibration*, 319(3–5):832 – 849, 2009.
- [16] M. Prandina, J.E. Mottershead, and E. Bonisoli. An assessment of damping identification methods. *Journal of Sound and Vibration*, 323(3–5):662 – 676, 2009.
- [17] S. H. Crandall. The role of damping in vibration theory. *Journal of Sound and Vibration*, 11(1), 1970.
- [18] R. H. Scanlan. Linear damping models and causality in vibrations. *Journal of Sound and Vibration*, 13(4):499–503, 1970.
- [19] G. B. Muravskii. On frequency independent damping. *Journal of Sound and Vibration*, 274(3–5):653–668, 2004.
- [20] V. Arora. Direct structural damping identification method using complex FRFs. *Journal of Sound and Vibration*, 339:304–323, 2015.
- [21] G.O. Ozgen and J.H. Kim. Direct identification and expansion of damping matrix for experimental-analytical hybrid modeling. *Journal of Sound and Vibration*, 308(1–2):348–372, 2007.
- [22] J.-L. Guyader. *Vibration in continuous media*. ISTE, Newport Beach, CA, 2006.
- [23] H.T. Banks and D.J. Inman. On damping mechanisms in beams. *Transaction of ASME, Journal of Applied Mechanics*, 58:716–723, 1991.

- [24] M.W.L.M. Rijnen, F. Pasteuning, R.H.B. Fey, G. van Schothorst, and H. Nijmeijer. A numerical and experimental study on viscoelastic damping of a 3d structure. *Journal of Sound and Vibration*, In Press, Corrected Proof.
- [25] 3M™ viscoelastic damping polymeres 112-130 technical data, 2012.
- [26] P. Cladé. *pyDAQmx: a Python interface to the National Instruments DAQmx driver*, 2015.
- [27] Polytec Portable Digital Vibrometer PDV 100 user manual, 2003.
- [28] P.E. Norman, G. Jung, C. Ratcliffe, R. Crane, and C. Davis. Development of an Automated Impact Hammer for Modal Analysis of Structures. Technical report, DSTO Defence Science and Technology Organisation, Australia, 2012.
- [29] J. Pribošek and J. Diaci. Electromagnetic microforging apparatus for low-cost fabrication of molds for microlens arrays. *Journal of Micromechanics and Microengineering*, 25(6):065018, 2015.
- [30] J. Woodhouse. Linear damping models for structural vibration. *Journal of Sound and Vibration*, 215(3):547 – 569, 1998.
- [31] F.E. Udewadia. A Note on Nonproportional Damping. *Journal of Engineering Mechanics*, 2009.
- [32] I.Y. Bar-Itzhack. Matrix Symmetrization. *Journal of Guidance, Control, and Dynamics*, 21(1):178–179, 1998.
- [33] A. Berman and W.G. Flannelly. Theory of Incomplete Models of Dynamic Structures. *AIAA Journal*, 9(8):1481–1487, 1971.
- [34] A. Berman. System identification of structural dynamic models – Theoretical and practical bounds. In *25th Structures, Structural Dynamics and Materials Conference*. AIAA, Palm Springs, CA, 1984.

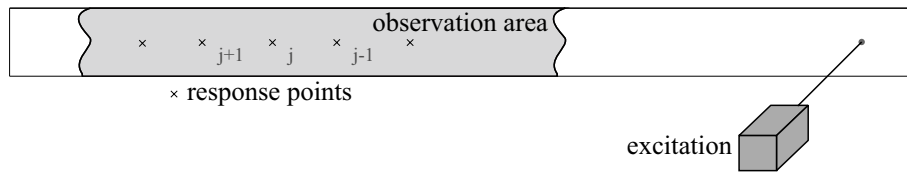


Figure 1: Local equation of motion method; excitation point and observation area.

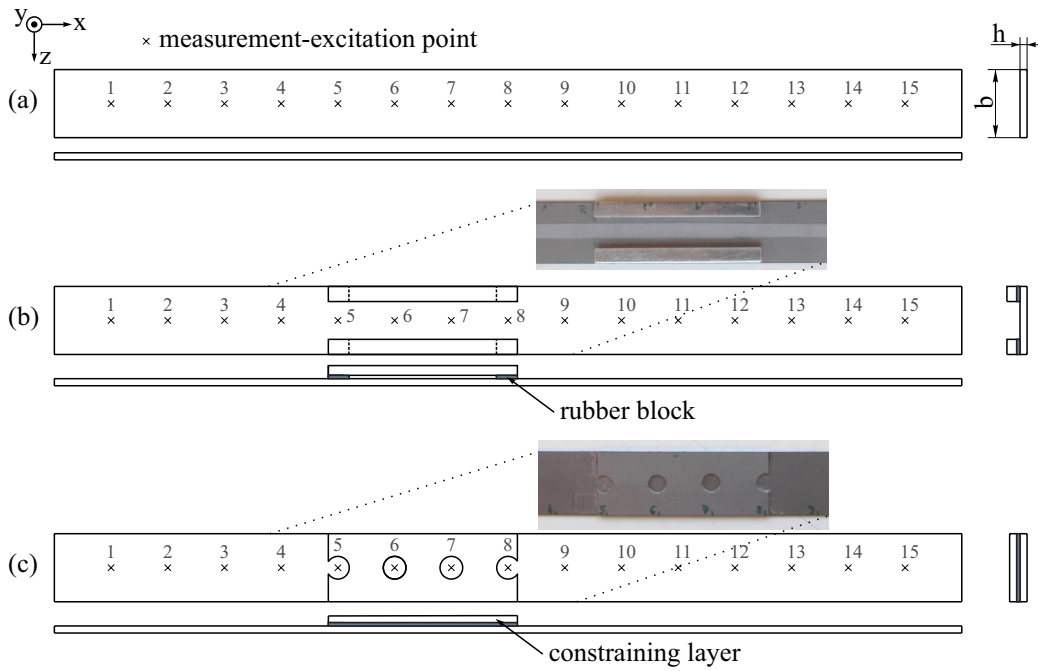


Figure 2: (a) plain beam specimen - beam A, (b) beam with added discrete viscous damper - beam B, (c) beam with added constrained layer damper - beam C

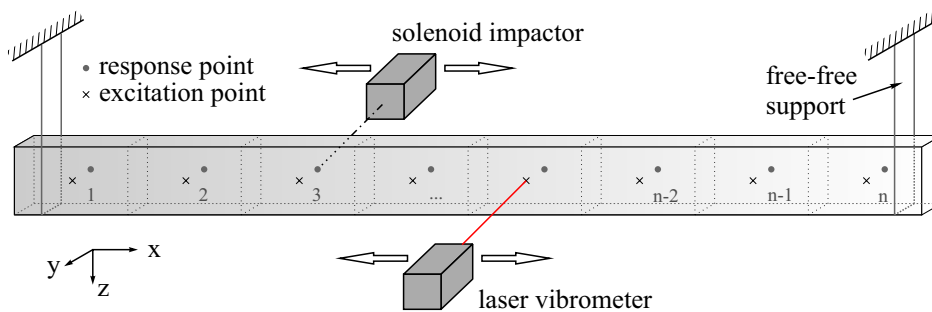


Figure 3: Measurement setup.

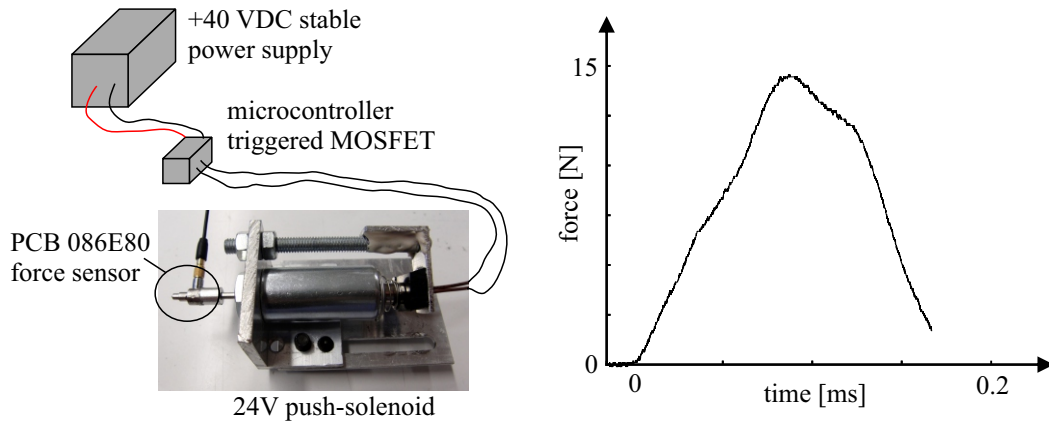


Figure 4: Detail of solenoid impactor with a typical excitation profile.

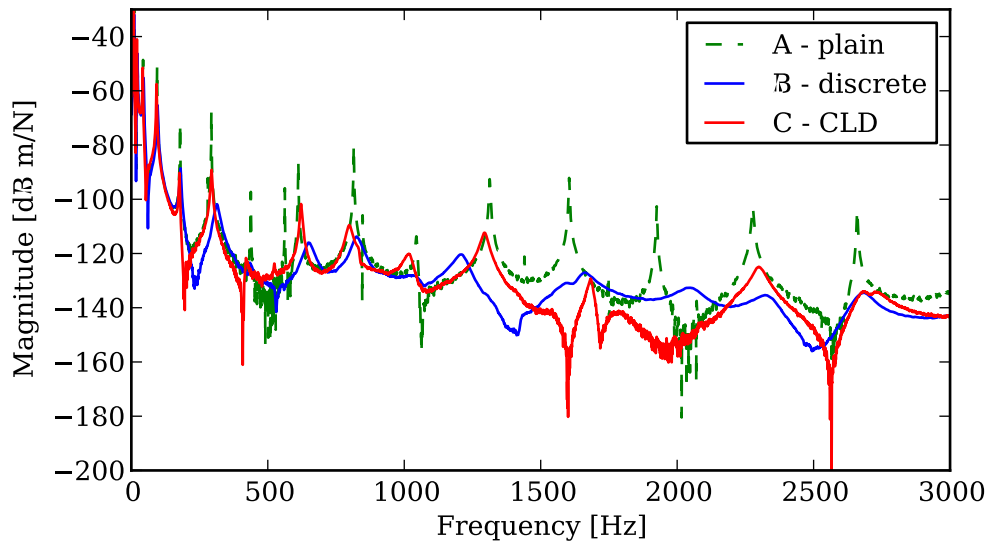


Figure 5: Receptance magnitude FRF plot for point 15-10.

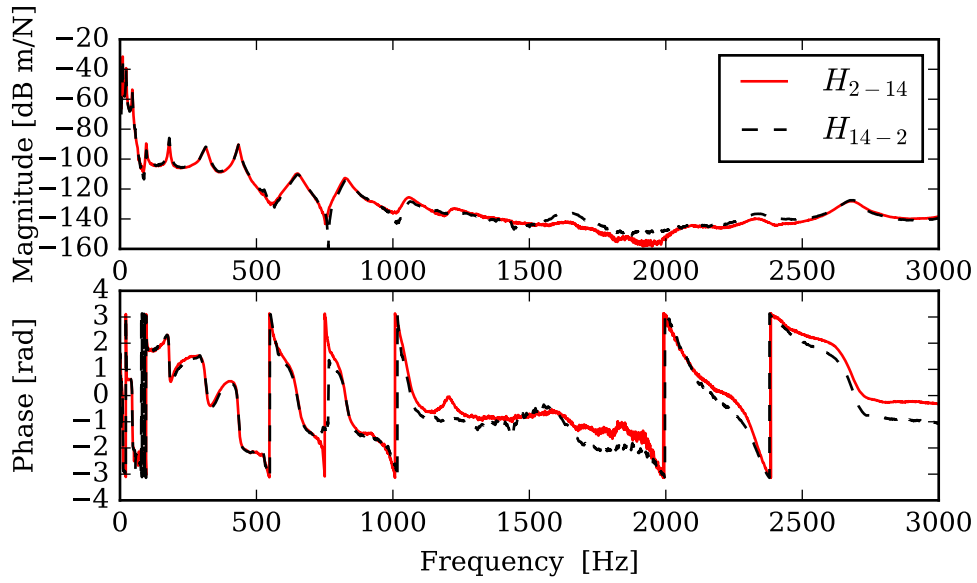


Figure 6: Reciprocity FRF plot for discretely damped beam B.

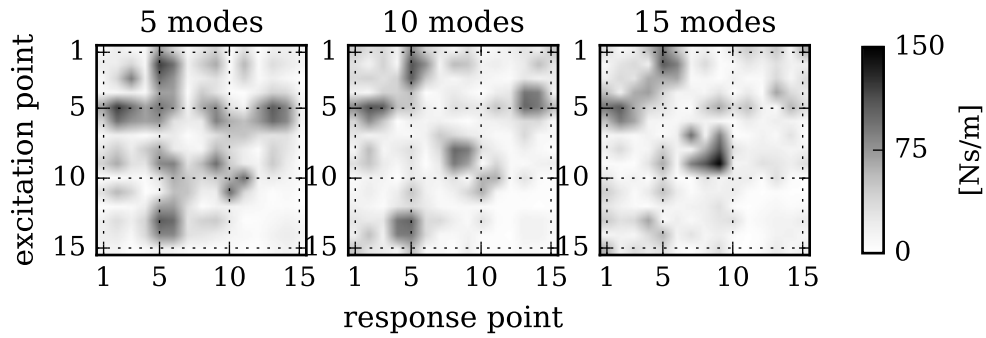


Figure 7: Identified absolute valued viscous-damping matrix for beam B, 5, 10 and 15 modes.

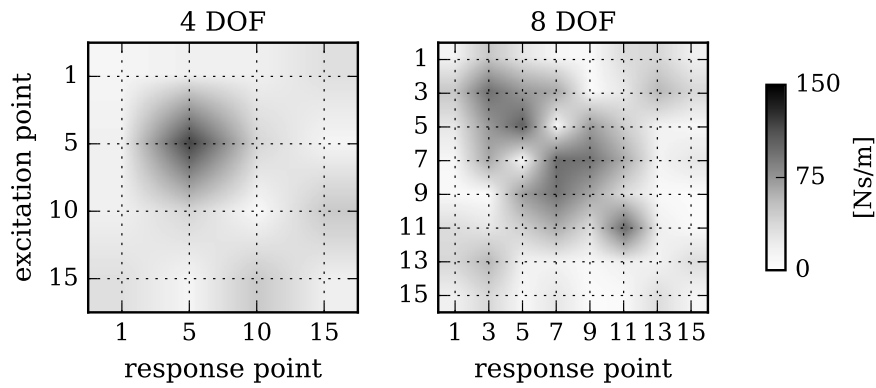


Figure 8: Identified absolute valued viscous-damping matrix for the beam B of the reduced FRF matrix.

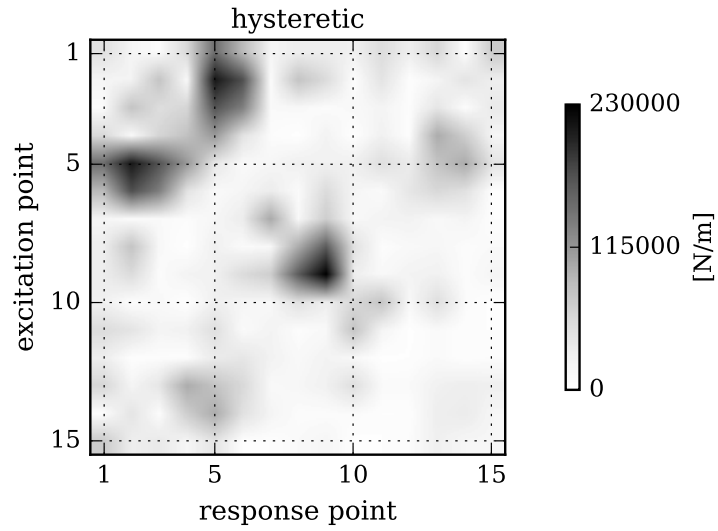


Figure 9: Identified absolute valued hysteretic-damping matrix for the discretely damped beam B.

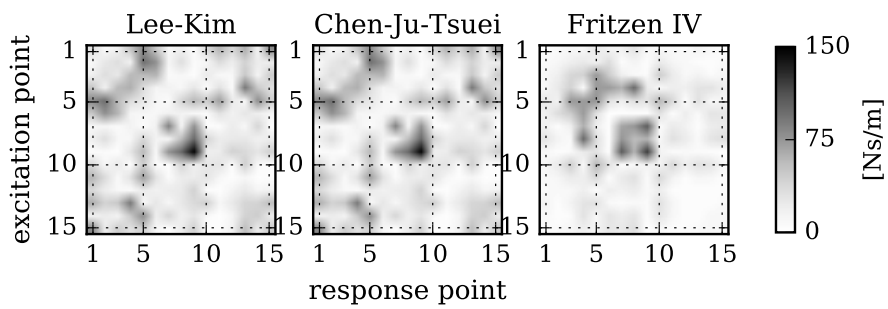


Figure 10: Identified absolute valued viscous-damping matrices for beam B.

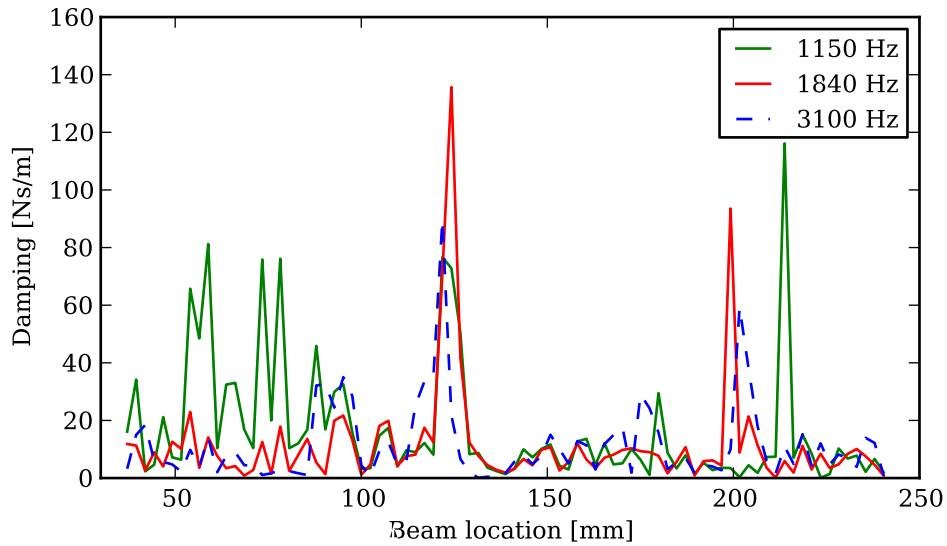


Figure 11: Identified absolute valued viscous damping for the local equation of motion for beam B at 1150, 1840 and 3100 Hz.

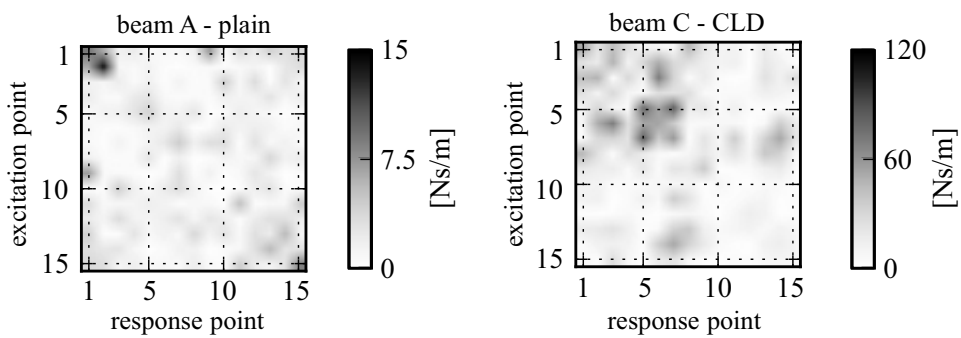


Figure 12: Identified absolute valued viscous-damping matrices for beams A and C. Please note the different scales.